Optimal Worm Shapes in a Caustic Environment

Sohyeon Park * Li-Tien Cheng † Bo Li ‡

May 30, 2017

Abstract

We study the optimal shapes flatworms take when they are placed in a caustic solution by introducing an energy model that takes a variational approach to optimal shapes. The context is the effect a caustic solution has on the worm exterior. Through variational calculus, we derive Euler-Lagrange equations and then a descent flow PDE for sending an initial worm shape to its minimum energy state. Numerically, we handle this PDE using finite difference methods and front tracking. Using simulations in different settings, we present further study of solutions under various conditions. The results using such a geometric and variational approach show promise in describing succinctly the ways that flatworms respond to caustic solutions in their environment.

1 Introduction

Invertebrate animals such as flatworms or roundworms have been commonly used in biomedical or related research since the 1800s. Ethical issues in animal testing have led scientists to choose invertebrate animals as alternatives to vertebrates in various experiments, such as with drug testing [11]. Invertebrate animals are important models not only because they can be good replacement for vertebrates for some experiments, but also because they possess numerous intriguing properties, such as great flexibility in changing their body shapes. For instance, a worm placed in a caustic solution sometimes exhibits abnormal movements and shapes in minimizing the amount of solution it touches. Previously, movement pattern analysis, using shape mode analysis, has been done among some physicists and biologists [10]. However, we are interested in writing mathematical models which can explain flatworms' movement and shape changes in response to caustic solutions, and specifically their responses to minimize the amount of the solution they touch.

*Department of Mathematics, University of California, San Diego, 9500 Gilman Drive, Mail code: 0112, La Jolla, CA 92093-0112, U.S.A. Email: sop009@ucsd.edu.

†Department of Mathematics, University of California, San Diego, 9500 Gilman Drive, Mail code: 0112, La Jolla, CA 92093-0112, U.S.A. Email: lcheng@math.ucsd.edu.

‡Department of Mathematics and NSF Center for Theoretical Biological Physics, University of California, San Diego, 9500 Gilman Drive, Mail code: 0112, La Jolla, CA 92093-0112, U.S.A. Email: bli@math.ucsd.edu.

We allow the worm to vary its shape about a central axis, but require it to preserve its enclosed volume. This translates geometrically to a minimization of the surface area of the worm with a fixed volume constraint. Since there are a variety of worms that are flat, we restrict ourselves to the simplified case of worms in two dimensions, and study minimization of perimeter with a fixed area constraint.We will develop a mathematical model for the worm and write down equations for the perimeter and area. Then, taking an energy-based approach, we will introduce an energy whose minimizers are our worm shapes of interest. This energy will make use of Lagrange multipliers to enforce the fixed area constraint. Variational calculus can be used to describe the minimizers of the energy and a flow-based gradient descent approach can be applied to generate a system of time dependent PDE's whose steady state solutions are the minimizers of interest. Numerically, we can solve these PDE's to approximate and construct the desired worm shapes, comparing them to theoretical results. for example, involving the isoperimetric inequality, when available, and study the dynamics involved [1].

2 Model

We model the worm body with two quantities: a curve, representing its central axis, and a radius, representing its width. Let $\gamma : [a, b] \to \mathbf{R}^2$ parametrically define the curve we call the central axis of the worm. Tangent and normal vectors of this curve can be defined by $\tau : [a, b] \to \mathbf{R}^2$ and $n : [a, b] \to \mathbf{R}^2$, respectively, where

$$\begin{aligned} \tau(s) &= \gamma'(s)/|\gamma'(s)| \\ n(s) &= (\tau(s))^{\perp}, \end{aligned}$$

for $s \in [a, b]$, and $[v_1, v_2]^{\perp} = [v_2, -v_1]$. We note here two useful identities: $(n(s))^{\perp} = -\tau(s)$ and $\tau(s) \cdot n(s) = 0$, or $\gamma'(s) \cdot n(s) = 0$.

Now given $r : [a, b] \to [0, \infty)$, we define the body of the worm by

$$B = \{\gamma(s) + Rn(s) | s \in [a, b], R \in [r(s), -r(s)]\}.$$

We call $r(s)$ the radius of the worm about its central axis. Note, in this setting, the worm boundary consists of the curves $\gamma(s) + Rn(s)$, for $s \in \{a, b\}, R \in [-r(s), r(s)]$, at its ends, and $\gamma(s) \pm r(s)n(s)$, for $s \in [a, b]$, along its sides. Since a general worm shape can be approximated by one satisfying the boundary conditions $r(a) = r(b) = 0$, we henceforth restrict our attention to this case.

Geometric quantities of interest to us include curvature of the central axis, length of the worm sides, and area of worm body. The curvature of the central axis plays a key role in the viability of our defined worm body. On the other hand, the length of worm sides, and its variations, are central to our application of minimizing the worm's contact with caustic material in the surrounding solution. Finally, the area of the worm body can be used to enforce the physical condition of a worm having fixed enclosed area while it deforms.

The standard definition of the curvature vector is the change of the tangent in the unit tangent direction: $\tau'(s)/\gamma'(s)$. This vector is normal to the curve, and its magnitude can be defined as the magnitude of the curvature. For the sign of the curvature, in the case where γ is a closed curve, the curvature is often defined as: curvature in the inward normal direction equals the curvature vector. We follow this to defined our signed curvature even for general $\gamma'(s)$:

$$H(s) = -\frac{\tau'(s)}{|\gamma'(s)|} \cdot n(s) = -\frac{1}{|\gamma'(s)|}(\gamma''(s) \cdot n(s)),$$

where the second equality uses $\gamma'(s) \cdot n(s) = 0$. We note here the useful identity,

$$\frac{n'(s)}{|\gamma'(s)|} = \frac{(\tau^{\perp}(s))'}{|\gamma'(s)|} = \frac{(\tau'(s))^{\perp}}{|\gamma'(s)|} = (-H(s)n(s))^{\perp} = H(s)\tau(s).$$

Now, if we study the change of coordinates from a point (x, y) in our worm body to (s, R) coordinates, defined by $[x, y]^T = \gamma(s) + Rn(s)$, we get the Jacobian matrix,

$$\frac{\partial(x, y)}{\partial(s, R)} = [\gamma'(s) + Rn'(s), n(s)]^T = [(1 + RH(s))|\gamma'(s)|\tau(s), n(s)]^T.$$

Then

$$\left|\det\left(\frac{\partial(x, y)}{\partial(s, R)}\right)\right| = |(1 + RH(s))|\gamma'(s)| \det[\tau(s), n(s)]| = |1 + RH(s)||\gamma'(s)|, \qquad (1)$$

since $[\tau(s), n(s)]$ has orthonormal columns and so is has absolute value of determinant 1. For a well-behaved change of coordinates, this quantity should be nonzero, which notably implies $1+RH(s) > 0$, for all $s \in [a, b]$, $R \in [-r(s), r(s)]$. This in turn translates to the requirement $|r(s)H(s)| < 1$. We thus require and only study worms that satisfy $|r(s)H(s)| < 1$, for all $s \in [a, b]$, meaning $1 \pm r(s)H(s) < 1$. Worm bodies that violate this condition impinge upon themselves for a nonphysical representation. This, by the way, is similar to the situation in geometrical optics concerning a wavefront forming swallowtails as it passes through itself.

The perimeter of the worm sides is the sum of the lengths of the curves representing each side, $\gamma(s) \pm r(s)n(s)$. These lengths are given by the expression

$$\int_a^b |(\gamma \pm rn)'(s)| \, ds.$$

Note, since

$$\begin{aligned}(\gamma \pm rn)'(s) &= \gamma'(s) \pm (r'(s)n(s) + r(s)n'(s)) \\ &= |\gamma'(s)|\tau(s) \pm (r'(s)n(s) + r(s)H(s)|\gamma'(s)|\tau(s)) \\ &= (1 \pm r(s)H(s))|\gamma'(s)|\tau(s) + r'(s)n(s),\end{aligned}$$

then

$$|(\gamma \pm rn)'(s)| = \sqrt{(1 \pm r(s)H(s))^2|\gamma'(s)|^2 + (r'(s))^2}.$$

We can thus write the perimeter as

$$P(\gamma, r) = \sum_{\pm} \int_a^b \sqrt{(1 \pm r(s)H(s))^2 |\gamma'(s)|^2 + (r'(s))^2}\, ds,$$

where $\sum_{\pm}$ sums together the contributions of the summand for each of the signs in $\pm$.

Let $C : \mathbf{R}^2 \to (0, \infty)$ denote the amount of caustic material in the solution. Then we also create a weighted perimeter that measures the amount of caustic material touching the worm sides:

$$\begin{aligned} WP(\gamma, r) &= \sum_{\pm} WP_{\pm} \\ &= \sum_{\pm} \int_a^b C(\gamma \pm rn) |(\gamma \pm rn)'(s)|\, ds \\ &= \sum_{\pm} \int_a^b C(\gamma \pm rn) \sqrt{(1 \pm r(s)H(s))^2 |\gamma'(s)|^2 + (r'(s))^2}\, ds. \end{aligned}$$

Note, in this simplified setting, we are not treating the surrounding solution as an incompressible fluid, but more as a background state.

The area enclosed by the worm body B is defined by

$$A(\gamma, r) = \int \int_B 1\, dxdy.$$

We expand this formula by changing coordinates: $[x, y] = \gamma(s) + Rn(s)$. Using (1), we get the expression

$$\begin{aligned} A(\gamma, r) &= \int_a^b \int_{-r(s)}^{r(s)} (1 + RH(s)) |\gamma'(s)|\, dRds \\ &= \int_a^b 2r(s) |\gamma'(s)|\, ds. \end{aligned}$$

Our goal is to find worm bodies and motions that seek to minimize the amount of caustic material the worm sides touch, while fixing the area of the worm body. We set this up in an energy incorporating our weighted perimeter and enclosed area, with a Lagrange multiplier for the area constraint:

$$E(\gamma, r, \lambda) = WP(\gamma, r) + \lambda(A(\gamma, r) - A_0), \tag{2}$$

where λ is a Lagrange multiplier, and A_0 is the desired enclosed area for the worm. We can then study the minimum of this energy, or variations of it that consider, for example, fixed γ, or a fixed r, or without area constraints, or satisfying various boundary conditions.

Note, in subsequent secitons, we will frequently suppress the dependence of γ and r on s, for simplicity of exposition.

3 Method

We plan to apply variational calculus on (2), and its variations, to calculate Euler-Lagrange equations and determine a descent flow for constructing minimizers. We first review variational calculus from the point of view of calculus of several variables, then go through a simple example from curve shortening, then apply variational calculus to our energy of interest, and finally present a descent flow for minimizing the energy.

3.1 Directional Derivatives

For a function of several variables, $f(x)$, the directional derivative of f at x in the direction of vector v is defined as $\nabla f(x) \cdot v$. An alternate definition of this directional derivative is

$$\left.\frac{d}{d\epsilon}\right|_{\epsilon=0} f(x+\epsilon v),$$

which essentially looks at the change of f when traveling with velocity v through x. Additionally, though a critical point of f can be defined as locations satisfying $\nabla f(x) = 0$, we can define it alternatively as locations x where the directional derivatives in all directions v are zero:

$$\left.\frac{d}{d\epsilon}\right|_{\epsilon=0} f(x+\epsilon v) = 0,$$

for all v. This alternate definition allows the concept of critical points to be extended from functions of several variables to the infinite dimensional case involving functionals such as our energy of interest.

3.2 Curve Shortening

For the case of functionals, we continue using our calculus terminology of critical points and directions. Consider the well-known example of curve shortening, where the functional to be minimized is the length of a smooth curve γ:

$$L(\gamma) = \int_a^b |\gamma'| \, ds.$$

Following the directional derivative definition, critical points γ satisfy

$$\frac{d}{d\epsilon} L(\gamma + \epsilon\tilde{\gamma}) = 0$$

for all directions $\tilde{\gamma}$ such that $\gamma + \epsilon\tilde{\gamma}$ are also the kind of curves we are interested in. In fact, it suffices to consider only normal directions, so we have $\tilde{\gamma} = \tilde{\gamma}_n n$ for $a < s < b$. Now,

$$\begin{aligned} \frac{d}{d\epsilon} L(\gamma + \epsilon\tilde{\gamma}) &= \int_a^b \frac{\gamma'}{|\gamma'|} \cdot \tilde{\gamma}' \, ds \\ &= -\int_a^b \left(\frac{\gamma'}{|\gamma'|}\right)' \cdot \tilde{\gamma} \, ds + \left[\frac{\gamma'}{|\gamma'|} \cdot \tilde{\gamma}\right]_a^b, \end{aligned}$$

using integration by parts in the last inequality. For the boundary terms, we consider the case

$$\left[\frac{\gamma'}{|\gamma'|}\cdot\tilde{\gamma}\right]_a^b = 0,$$

which occurs, for example, when we restrict our attention to curves whose endpoints are fixed, so $\gamma(s) = (\gamma + \epsilon\tilde{\gamma})(s)$ at $s = \{a, b\}$, and $\tilde{\gamma}(s) = 0$ at $s = \{a, b\}$. Then the directional derivative satisfies

$$\frac{d}{d\epsilon}L(\gamma + \epsilon\tilde{\gamma}) = -\int_a^b \left(\frac{\gamma'}{|\gamma'|}\right)'\cdot\tilde{\gamma}\ ds = -\int_a^b \left[\left(\frac{\gamma'}{|\gamma'|}\right)'\cdot n\right]\tilde{\gamma}_n\ ds = \int_a^b H|\gamma'|\tilde{\gamma}_n\ ds. \tag{3}$$

Then critical points satisfy

$$-\int_a^b H|\gamma'|\tilde{\gamma}_n\ ds = 0,$$

and, since this is for all $\tilde{\gamma}_n$, this translates to $H|\gamma'| = 0$, or, more geometrically, $H = 0$. This is known as the Euler-Lagrange equation for the functional.

From (3), we can also choose a normal component $\tilde{\gamma}_n n$ that decreases the length:

$$\frac{d}{d\epsilon}L(\gamma + \epsilon\tilde{\gamma}_n n) < 0, \tag{4}$$

when γ is not a critical point. A simple choice is $\tilde{\gamma}_n = -H|\gamma'|$, since then

$$\frac{d}{d\epsilon}L(\gamma + \epsilon\tilde{\gamma}_n n) = -\int_a^b H^2|\gamma'|^2\ ds < 0,$$

when γ is not a critical point; however, a more geometric choice that satisfies (4), and one that is independent of the parametrization of γ, includes an additional $1/|\gamma'|$: $\tilde{\gamma}_n = -H$. We can use this direction for a flow-based method minimizing the functional. Let $\gamma = \gamma(s, t)$ now additionally depend on time, with given $\gamma(s, t = 0)$, the initial curve. Then we consider flow in our chosen direction:

$$\gamma_t = -Hn,$$

which is known as curvature flow, and which will decrease the energy until it reaches a critical point, at which point $\gamma_t = 0$ and it stops.

We end by summarizing the curve shortening process, so we can follow similar steps for our energy of interest:

1. Take the directional derivative of the energy and simplify it, using, for example, integration by parts, into the form
$$\int_a^b G\cdot\tilde{\gamma}\ ds,$$
where $\tilde{\gamma} = \tilde{\gamma}_n n$.

2. Set it equal to zero and simplify for the Euler-Lagrange equation: $G \cdot n = 0$;

3. Choose a descent flow on the energy of the form

$$\gamma_t = -\frac{G \cdot n}{|\gamma_s|} n.$$

3.3 Euler-Lagrange Equations

We handle the directional derivative of our energy of interest in parts:

$$\begin{aligned}
\left.\frac{d}{d\epsilon}\right|_{\epsilon=0} E(\gamma + \epsilon\tilde{\gamma}, R + \epsilon\tilde{R}) &= \left.\frac{d}{d\epsilon}\right|_{\epsilon=0} WP(\gamma + \epsilon\tilde{\gamma}, R + \epsilon\tilde{R}) + \lambda \left.\frac{d}{d\epsilon}\right|_{\epsilon=0} A(\gamma + \epsilon\tilde{\gamma}, R + \epsilon\tilde{R}) \\
&= \sum_{\pm} \left.\frac{d}{d\epsilon}\right|_{\epsilon=0} WP_{\pm}(\gamma + \epsilon\tilde{\gamma}, R) + \lambda \left.\frac{d}{d\epsilon}\right|_{\epsilon=0} A(\gamma + \epsilon\tilde{\gamma}, R) + \\
&\quad \sum_{\pm} \left.\frac{d}{d\epsilon}\right|_{\epsilon=0} WP_{\pm}(\gamma, R + \epsilon\tilde{R}) + \lambda \left.\frac{d}{d\epsilon}\right|_{\epsilon=0} A(\gamma, R + \epsilon\tilde{R}).
\end{aligned}$$

For simplicity, we assume γ has fixed endpoints and γ' satisfies free boundary conditions, in other words, $\gamma''(a) = \gamma''(b) = 0$. With these boundary conditions, we will simplify each term of the directional derivative separately, to get an expression of the form

$$\sum_{\pm} \int_a^b G_{WP_{\pm},\gamma} \cdot \tilde{\gamma}\ ds + \lambda \int_a^b G_{A,\gamma} \tilde{r}\ ds + \sum_{\pm} \int_a^b G_{WP_{\pm},r} \cdot \tilde{\gamma}\ ds + \lambda \int_a^b G_{A,r} \tilde{r}\ ds.$$

We present the terms in increasing order of complexity, with $G_{A,r}$ first, then $G_{A,\gamma}$, then $G_{WP_{\pm},R,\pm}$, and finally $G_{WP_{\pm},\gamma,\pm}$. Additionally, since the computation of the last term is quite involved, we defer its details to the appendix.

We handle $G_{A,r}$ first, as it is the simplest. The directional derivative in this case is

$$\left.\frac{d}{d\epsilon}\right|_{\epsilon=0} A(\gamma, R + \epsilon\tilde{R}) = 2\int_a^b \tilde{r}|\gamma'|\ ds = 2\int_a^b |\gamma'|\tilde{r}\ ds,$$

which implies $G_{A,r} = 2|\gamma'|$.

Next in complexity is $G_{A,\gamma}$. The directional derivative in this case is

$$\begin{aligned}
\left.\frac{d}{d\epsilon}\right|_{\epsilon=0} A(\gamma + \epsilon\tilde{\gamma}, R) &= 2\int_a^b r\frac{\gamma'}{|\gamma'|} \cdot \tilde{\gamma}'\ ds \\
&= -2\int_a^b (r\tau)' \cdot \tilde{\gamma}\ ds + 2\left[r\tau \cdot \tilde{\gamma}\right]_a^b,
\end{aligned}$$

however, note that $r(a) = r(b) = 0$. This then implies

$$G_{A,\gamma} = -2(r\tau)'.$$

Next in complexity is $G_{WP_{\pm},r}$. To reduce the length of the formulas, we we introduce the notation $C_\pm = C(\gamma \pm rn)$ and $D_\pm = \sqrt{(1 \pm rH)^2|\gamma'|^2 + (r')^2}$. Then the directional derivative in this case is

$$\begin{aligned}
&\frac{d}{d\epsilon}\Big|_{\epsilon=0} \int_a^b C(\gamma \pm (r+\epsilon\tilde{r})n)\sqrt{(1 \pm (r+\epsilon\tilde{r})H)^2|\gamma'|^2 + (r'+\epsilon\tilde{r}')^2}\; ds \\
&= \pm \int_a^b \left(\nabla C_\pm \cdot n + \frac{C_\pm}{D_\pm}(1 \pm rH)|\gamma'|^2 H \right) \tilde{r}\; ds + \int_a^b \frac{C_\pm}{D_\pm} r'\tilde{r}'\; ds \\
&= \pm \int_a^b \left(\nabla C_\pm \cdot n + \frac{C_\pm}{D_\pm}(1 \pm rH)|\gamma'|^2 H \right) \tilde{r}\; ds - \int_a^b \left(\frac{C_\pm}{D_\pm} r' \right)' \tilde{r}\; ds + \left[\frac{C_\pm}{D_\pm} r'\tilde{r} \right]_a^b,
\end{aligned}$$

however, note $\tilde{r}(a) = \tilde{r}(b) = 0$ so that $r + \epsilon\tilde{r}$ satisfies zero boundary conditions at the endpoints. This then implies

$$G_{WP_{\pm},r} = \pm \left(\nabla C_\pm \cdot n + \frac{C_\pm}{D_\pm}(1 \pm rH)|\gamma'|^2 H \right) - \left(\frac{C_\pm}{D_\pm} r' \right)'.$$

Finally, we present the results in the case $G_{WP_{\pm},\gamma}$, with details in the appendix. The result of the directional derivative is

$$\begin{aligned}
&\frac{d}{d\epsilon}\Big|_{\epsilon=0} \int_a^b C(\gamma + \epsilon\tilde{\gamma} \pm rn)\sqrt{(1 \pm rH(\gamma+\epsilon\tilde{\gamma}))^2|\gamma' + \epsilon\tilde{\gamma}|^2 + (r')^2}\; ds \\
&= \mp \int_a^b \left(\frac{C_\pm}{D_\pm}(1 \pm rH) rn \right)'' \cdot \tilde{\gamma}\; ds \mp \int_a^b \left[\frac{C_\pm}{D_\pm}(1 \pm rH) r \left(\frac{(\gamma'' \cdot \tau)n}{|\gamma'|} - 2H|\gamma'|\tau \right) \right]' \cdot \tilde{\gamma}\; ds \\
&\quad - \int_a^b \left(\frac{C_\pm}{D_\pm}(1 \pm rH)^2 \gamma' \right)' \cdot \tilde{\gamma}\; ds + \int_a^b D_\pm \nabla C_\pm \cdot \tilde{\gamma} \pm \int_a^b \left(D_\pm \frac{r(\nabla C_\pm)^\perp}{|\gamma'|} \right)' \cdot \tilde{\gamma} \\
&\quad \pm \int_a^b \left(D_\pm \frac{r \nabla C_\pm \cdot n}{|\gamma'|} \tau \right)' \cdot \tilde{\gamma}\; ds \pm \left[\frac{C_\pm}{D_\pm} r'(n \cdot \tilde{\gamma}) \right]_a^b + \left[\frac{C_\pm}{D_\pm} \gamma' \cdot \tilde{\gamma} \right]_a^b
\end{aligned}$$

which, under our boundary conditions on the curve, implies

$$\begin{aligned}
G_{WP_{\pm},\gamma} \;=\; & \mp \left(\frac{C_\pm}{D_\pm}(1 \pm rH) rn \right)'' \mp \left[\frac{C_\pm}{D_\pm}(1 \pm rH) r \left(\frac{(\gamma'' \cdot \tau)n}{|\gamma'|} - 2H|\gamma'|\tau \right) \right]' \\
& - \left(\frac{C_\pm}{D_\pm}(1 \pm rH)^2 \gamma' \right)' + D_\pm \nabla C_\pm \pm \left(D_\pm \frac{r(\nabla C_\pm)^\perp}{|\gamma'|} \right)' \quad \pm \left(D_\pm \frac{r \nabla C_\pm \cdot n}{|\gamma'|} \tau \right)'.
\end{aligned}$$

We note that the expressions presented in this case are only partially simplified, for length, and there may be further simplifications that shed more light on the geometric significance of some of the terms.

Altogether, the results for these terms combine to give the Euler-Lagrange equations:

$$\begin{aligned}
\sum_\pm (G_{WP_{\pm},\gamma} \cdot n) + \lambda(G_{A,\gamma} \cdot n) &= 0 \\
\sum_\pm (G_{WP_{\pm},r} \cdot n) + \lambda(G_{A,r} \cdot n) &= 0.
\end{aligned}$$

3.4 Descent Flow

We can then write out the descent flow for our energy, letting $\gamma = \gamma(s,t)$ depend on time and switching to partial derivative notation:

$$\begin{aligned} \gamma_t &= -\sum_{\pm}\left(\frac{G_{WP_{\pm},\gamma}}{|\gamma_s|}\cdot n\right) - \lambda\left(\frac{G_{A,\gamma}}{|\gamma_s|}\cdot n\right) \\ r_t &= -\sum_{\pm}\left(\frac{G_{WP_{\pm},r}}{|\gamma_s|}\cdot n\right) - \lambda\left(\frac{G_{A,r}}{|\gamma_s|}\cdot n\right), \end{aligned} \tag{5}$$

where each term simplifies as follows:

$$\begin{aligned} -\frac{G_{WP_{\pm},\gamma}}{|\gamma_s|}\cdot n &= \pm\frac{1}{|\gamma_s|}\left(\frac{C_{\pm}}{D_{\pm}}(1\pm rH)r\right)_{ss} \pm \frac{1}{|\gamma_s|}\left(\frac{C_{\pm}}{D_{\pm}}(1\pm rH)r\frac{\gamma_{ss}\cdot\tau}{|\gamma_s|}\right)_s \\ &\quad -\frac{C_{\pm}}{D_{\pm}}(1\pm rH)H|\gamma_s| - (1\mp rH)D_{\pm}\frac{\nabla C_{\pm}\cdot n}{|\gamma_s|} \mp \frac{1}{|\gamma_s|}\left(rD_{\pm}\frac{\nabla C_{\pm}}{|\gamma_s|}\right)_s\cdot\tau \\ -\frac{G_{A,\gamma}}{|\gamma_s|}\cdot n &= -rH \\ -\frac{G_{WP_{\pm},r}}{|\gamma_s|} &= \frac{1}{|\gamma_s|}\left(\frac{C_{\pm}}{D_{\pm}}r_s\right)_s \mp \left(\frac{\nabla C_{\pm}\cdot n}{|\gamma_s|} + \frac{C_{\pm}}{D_{\pm}}(1\pm rH)|\gamma_s|H\right) \\ -\frac{G_{A,r}}{|\gamma_s|} &= -2. \end{aligned}$$

We provide details of the first identity in the appendix and again note that the expressions presented in this case are only partially simplified, for length.

Also, from these terms, we can form the descent flow for several other subcases [6]. We explicitly write out and analyze two of them here: the case where γ is given and fixed and with no area constraint,

$$r_t = -\sum_{\pm}\left(\frac{G_{WP_{\pm},r}}{|\gamma_s|}\cdot n\right), \tag{6}$$

and the case where r is given and fixed and with no area constraint,

$$\gamma_t = -\sum_{\pm}\left(\frac{G_{WP_{\pm},\gamma}}{|\gamma_s|}\cdot n\right) - \lambda\left(\frac{G_{A,\gamma}}{|\gamma_s|}\cdot n\right). \tag{7}$$

Studying the parabolicity of (6), we note the largest derivative term in r on the right hand side is r_{ss}. We compute the coefficient of r_{ss} to be

$$\frac{1}{|\gamma_s|}\sum_{\pm}\left(\frac{C_{\pm}}{D_{\pm}} - \frac{C_{\pm}}{D_{\pm}^3}(r_s)^2\right) = \sum_{\pm}\frac{C_{\pm}}{D_{\pm}^3}(1+rH)^2|\gamma_s| > 0.$$

In fact, it is bounded below by a constant that is greater than zero. Thus, the PDE is parabolic.

Studying the parabolicity of (7), we note the largest derivative term in γ on the right hand side is γ_{ssss}. We compute the coefficient matrix of γ_{ssss} to be

$$\frac{1}{|\gamma_s|}\sum_{\pm}\left(-\frac{C_\pm}{D_\pm}\frac{r^2}{|\gamma_s|}+\frac{C_\pm}{D_\pm^3}(1\pm rH)^2r^2|\gamma_s|\right)(n\otimes n)=-\sum_{\pm}\frac{C_\pm}{D_\pm^3}\frac{(rr_s)^2}{|\gamma_s|^2}(n\otimes n),$$

where $n\otimes n$ refers to the tensor product between the vectors n and itself. This matrix has two eigenvalues, 0 and

$$-\sum_{\pm}\frac{C_\pm}{D_\pm^3}\frac{(rr_s)^2}{|\gamma_s|^2}\leq 0.$$

Thus, the PDE is degenerate parabolic when $r, r_s \neq 0$, but does degenerate further when $r = 0$ or $r_s = 0$.

3.5 Lagrange Multiplier

For the enclosed area constraint, we also use a flow-based approach on λ, so $\lambda = \lambda(t)$. Then, after requiring the initial worm body to have the desired enclosed area, we use λ to preserve this area during the flow: $\partial A/\partial t = 0$. Taking a time derivative of the area gives:

$$\begin{aligned}\frac{\partial A}{\partial t} &= 2\int_a^b |\gamma_s| r_t\ ds - 2\int_a^b \left(r\frac{\gamma_s}{|\gamma_s|}\right)_s\cdot\gamma_t\ ds\\ &= -2\int_a^b\left(\sum_{\pm}G_{WP_\pm,r}+\lambda G_{A,r}\right)\ ds - 2\int_a^b\left(\sum_{\pm}G_{WP_\pm,\gamma}+\lambda G_{A,\gamma}\right)rH\ ds.\end{aligned}$$

Setting this equal to zero and solving for λ gives

$$\lambda=\frac{\sum_\pm\int_a^b G_{WP_\pm,r}\ ds+\sum_\pm\int_a^b G_{WP_\pm,\gamma}rH\ ds}{\int_a^b G_{A,r}\ ds+\int_a^b G_{A,\gamma}rH\ ds}. \tag{8}$$

4 Numerical Approximations

We handle the system of PDE's (5) in a finite difference framework, with the method of lines and finite difference approximation formulas for parabolic PDE's. We first detail the basic procedure on the well-known heat equation and biharmonic equation, then apply it to our system of PDE's [2, 5].

4.1 Heat and Biharmonic Equations

Consider, the heat equation with $K > 0$, for parabolicity, given by

$$u_t(x,t) = Ku_{xx}(x,t),$$

for $x \in [a,b], t > 0$, with boundary conditions, such as Dirichlet or von Neumann, given at $x = a, b$, and given initial condition, $u(x, t = 0)$. Laying down a uniforms grid, with equally spaced nodes at x_i, $i = 0, \ldots, N$, let $u_i(t)$ denote our approximation of $u(x_i, t)$. Then we can apply a second order central differencing approximation to $u_{xx}(x_i, t)$:

$$u_{xx}(x_i, t) \approx \frac{u_{i+1}(t) - 2u_i(t) + u_{i-1}(t)}{h^2},$$

where h denotes the stepsize of the grid. This equation should, of course, be modified near the boundaries of the interval $[a, b]$ to incorporate the given boundary conditions, since $u_{i+1}(t)$ and $u_{i-1}(t)$ may refer to locations lying outside $[a, b]$. Thus, the heat equation at (x_i, t) is approximated by the equation

$$(u_i)_t(t) = K\frac{u_{i+1}(t) - 2u_i(t) + u_{i-1}(t)}{h^2},$$

which, since there are no more derivatives in x, is a system of ODE's.

Now, we select an appropriate ODE solver, such as Euler's method. For this method, we lay down a grid in time with nodes at t_k, $k = 0, \ldots, M$, and let $u_i^{(k)}$ denote our approximation of $u_i(t_k)$, which, in turn, approximates $u(x_i, t_k)$. Then applying a first order forward differencing approximation to $(u_i)_t(t_k)$:

$$(u_i)_t(t_k) \approx \frac{u^{(k+1)} - u^{(k)}}{\Delta t_k},$$

where $\Delta t_k = t(k+1) - t(k)$, our system of ODE's becomes

$$\frac{u_i^{(k+1)} - u_i^{(k)}}{\Delta t_k} = K\frac{u_{i+1}^{(k)} - 2u_i^{(k)} + u_{i-1}^{(k)}}{h^2}.$$

This is usually written as

$$u_i^{(k+1)} = u_i^{(k)} + K\Delta t_k \left(\frac{u_{i+1}^{(k)} - 2u_i^{(k)} + u_{i-1}^{(k)}}{h^2} \right), \tag{9}$$

which allows us to advance a time step.

Convergence of the approximations generated from (9) to the true solution depends on consistency and stability. A full analysis of stability, using von Neumann analysis, reveals a restriction on the size of the stepsize in time, known as the CFL condition: the largest possible stepsize giving stability is $\Delta t_k = h^2/(2K)$. With this choice of stepsize, the approximations generated from (9) are second order accurate in space.

Similarly, the biharmonic equation, this time with $K < 0$, for parabolicity, is

$$u_t(x, t) = Ku_{xxxx}(x, t),$$

for $x \in [a,b], t > 0$, and it can be discretized, using Euler's method in time and second order central differencing of u_{xxxx} in space, as

$$u_i^{(k+1)} = u_i^{(k)} + K\Delta t_k \left(\frac{u_{i+2}^{(k)} - 4u_{i+1}^{(k)} + 4u_i^{(k)} - 4u_{i-1}^{(k)} + u_{i-2}^{(k)}}{h^4} \right),$$

where there are suitable boundary conditions at a, b. A stability analysis in this case shows that the largest time step for stability is $\Delta t_k = h^4/(-8K)$.

4.2 Numerical Descent Flow

For our descent flow (5), we lay down a uniform grid over $[a,b]$, with equally spaced nodes s_i. Writing

$$\begin{aligned}
(\gamma_i)_t &= -\left[\sum_{\pm} \left(\frac{G_{WP_{\pm},\gamma}}{|\gamma_s|} \cdot n \right) + \lambda \left(\frac{G_{A,\gamma}}{|\gamma_s|} \cdot n \right) \right]_i \\
(r_i)_t &= -\left[\sum_{\pm} \left(\frac{G_{WP_{\pm},r}}{|\gamma_s|} \cdot n \right) - \lambda \left(\frac{G_{A,r}}{|\gamma_s|} \cdot n \right) \right]_i,
\end{aligned}$$

we can approximate the right hand sides by first expanding so that they are written in terms of $\gamma, r, \gamma_s, r_s, \gamma_s, r_{ss}, \gamma_{ss}, r_{sss}, \gamma_{sss}, \gamma_{ssss}$, then using central differencing approximations on these derivatives:

$$\begin{aligned}
(u_s)_i &\approx \frac{u_{i+1} - u_{i-1}}{2h} \\
(u_{ss})_i &\approx \frac{u_{i+1} - 2u_i + u_{i-1}}{h^2} \\
(u_{sss})_i &\approx \frac{u_{i+2} - 2u_{i+1} + 2u_{i-1} - u_{i-2}}{2h^3} \\
(u_{ssss})_i &\approx \frac{u_{i+2} - 4u_{i+1} + 4u_i - 4u_{i-1} + u_{i-2}}{h^4},
\end{aligned}$$

with $u = r$ or $u = \gamma_j$, for $j = 1, 2$, giving a systems of ODE's. This procedure, in the context of curves such as our γ, is known as front tracking, since discrete points are placed on the curve, or front, and then followed, or tracked, in time [6, 8, 9]. Finally, with Euler's method discretizing in time, we can write our approximation scheme as

$$\begin{aligned}
\gamma_i^{(k+1)} &= \gamma_i^{(k)} - \Delta t_k \left[\sum_{\pm} \left(\frac{G_{WP_{\pm},\gamma}}{|\gamma_s|} \cdot n \right) + \lambda \left(\frac{G_{A,\gamma}}{|\gamma_s|} \cdot n \right) \right]_i^{(k)} \\
r_i^{(k+1)} &= r_i^{(k)} - \Delta t_k \left[\sum_{\pm} \left(\frac{G_{WP_{\pm},r}}{|\gamma_s|} \cdot n \right) - \lambda \left(\frac{G_{A,r}}{|\gamma_s|} \cdot n \right) \right]_i^{(k)}.
\end{aligned} \tag{10}$$

At each time step k, $\lambda^{(k)}$ can be solved through numerical quadrature on (8). In our case, we use the midpoint rule, since it is an open Newton-Cotes formula and hence avoids endpoints, where there are more restrictions for finite difference approximations. Furthermore,

the CFL condition should be approximately determined by the coefficient of the highest order terms r_{ss} and γ_{ssss}. From our previous analysis in section 3.4, for γ fixed and no area constraint, we try $\Delta t_k = h^2/(2M_r^{(k)})$, or slightly smaller, where central differencing is used to approximate

$$M_r^{(k)} = \max_i \left[\sum_{\pm} \frac{C_{\pm}}{D_{\pm}^3} (1 \pm rH)^2 |\gamma_s| \right]_i^{(k)},$$

and, for r fixed and no area constraint, we try $\Delta t_k = h^4/(8M_\gamma^{(k)})$, or slightly smaller, where central differencing is used to approximate

$$M_\gamma^{(k)} = \max_i \left[\sum_{\pm} \frac{C_{\pm}}{D_{\pm}^3} \frac{(rr_s)^2}{|\gamma_s|^2} \right]_i^{(k)}.$$

For our general case of (5), we try the combination

$$\Delta t_k = h^4/(8M_\gamma^{(k)} + 2h^2 M_r^{(k)}), \tag{11}$$

or slightly smaller. Stability in these cases, with these choices of time stepsize, is verified numerically.

We summarize the final algorithm as follows:

1. Lay down a uniform grid in $[a, b]$ with stepsize h;
2. Set $k = 0$ and start with an initial worm shape given discretely as $\gamma_i^{(0)}, r_i^{(0)}$;
3. Solve for $\lambda^{(k)}$ using midpoint rule on (8);
4. Form Δt_k according to (11);
5. Generate $\gamma_i^{(k+1)}$ and $r_i^{(k+1)}$ according to (10), thus advancing a time step;
6. Set $k = k + 1$ and return to step 3.

5 Results

We run numerical simulations of our algorithm to view and check optimal worm shapes and dynamics.

We begin with a verification of results. When $C \equiv 1$, the homogeneous case, the weighted perimeter is simply the perimeter. In this case, the optimal worm shape is known, as a consequence of isoperimetric inequality, to have a straight line for central axis and worm sides that are arcs of circles. We take as initial worm shape

$$\begin{aligned} \gamma(s,0) &= \left[s, \frac{1}{2}\sin(\pi s) \right]^T \\ r(s,0) &= \frac{1}{10}\sin(\pi s)\left(\frac{9}{10} + \frac{1}{10}\cos(10\pi s) \right), \end{aligned}$$

for $s \in [0,1]$, which has enclosed area calculated approximately as $A_0 = 0.151436966015541$ using central differencing and the midpoint rule. For the worm side on top, the exact solution should be an arc from the circle of radius $\rho = 1.167845974989029$, an approximation we obtain from the secant method solving

$$\left(\frac{A_0}{2} - \rho^2 \arcsin\frac{1}{2\rho}\right)^2 - \frac{1}{4}\left(\rho^2 - \frac{1}{4}\right) = 0,$$

and centered approximately at $(0.5, -1.055397660267482)$. We plot the final and converged worm shape, computed by our algorithm using $N = 80$ subdivisions in our grid and $200,000$ time steps, along with this circle in figure 1. Note the top side of the worm lies virtually on top of the circle. Furthermore, we compute $1.570847661858110 \cdot 10^{-5}$ as the maximum distance the points of the top side of the worm lie away from the circle. With $N = 40$, this maximum distance is $4.028649836265163 \cdot 10^{-4}$, which shows our results improve with smaller stepsizes h, hinting at convergence as h goes to zero.

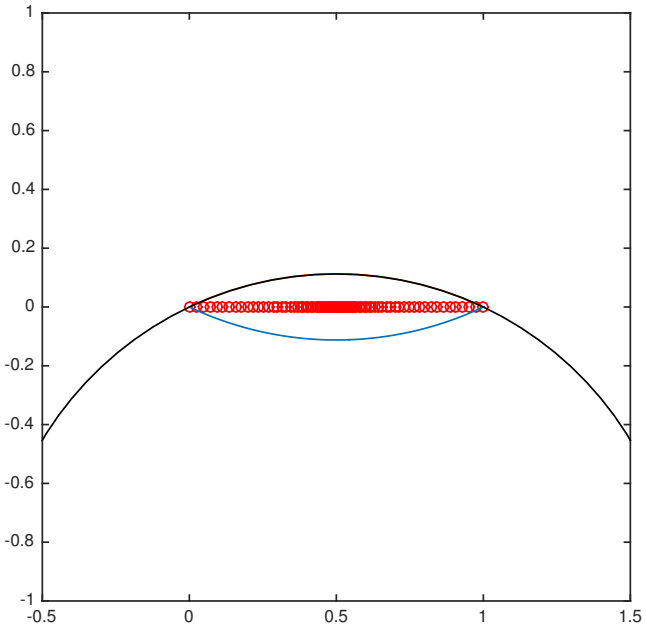

Figure 1: This figure shows optimal worm shape in a homogeneous solution. Overlayed is a circle whose arc gives the exact solution, from isoperimetric inequality, for the top side of the worm.

We then show the details of the dynamics and optimal worm shape for a more complicated example, when

$$C(x,y) = \frac{3}{5} + \frac{2}{5}\sin(2\pi x)\sin(2\pi y).$$

In figure 2, we show the initial worm shape, given by

$$\begin{aligned} \gamma(s,0) &= [s, s^2]^T \\ r(s,0) &= \frac{1}{10}\sin(\pi s)\left(\frac{9}{10} + \frac{1}{10}\cos(10\pi s)\right), \end{aligned}$$

for $s \in [0,1]$, followed by our computed worm shapes, for $N = 100$, at different times. Note, the worm quickly loses the initial waviness in its sides by the next plotted time step. The plots also show it deforming so its sides are away from yellow background areas that denote larger C, and into purple areas that denote smaller C, at subsequent time steps. In figure 3, the energy plot shows decrease and convergence of the energy, while the area plot shows the area being approximately preserved during the flow, with relative error around 0.1%.

We then show two more results of optimal worm shape, for $N = 100$, under the same C but different worm end locations and different enclosed area. We chose a thin worm, in one case, with small enclosed area, using initial worm shape

$$\begin{aligned} \gamma(s,0) &= \left[\frac{2}{5}\sin(\pi s), \frac{7}{10}\cos(\pi s)\right]^T \\ r(s,0) &= \frac{1}{40}\sin(\pi s), \end{aligned}$$

for $s \in [0,1]$, with final converged worm shape shown in figure 4. We then chose a long worm in the other case, with endpoints further away, using initial worm shape

$$\begin{aligned} \gamma(s,0) &= [-1 + 2s, 0]^T \\ r(s,0) &= \frac{3}{40}\sin(\pi s), \end{aligned}$$

for $s \in [0,1]$, with final converged worm shape shown in figure 4. Note, the worm sides settle closer to purple regions and away from yellow regions. In both cases, the energy decreased up until convergence, with the area approximately preserved.

We finally show two results from subcases, the first where γ is given and fixed, and the second where r is given and fixed and, additionally, without area constraint. Figure 5 shows the resulting optimal worm shapes in these cases for the same C and $N = 100$. Note, other subcases that remove the area constraint frequently exhibit the optimal worm to be infinitesimally thin.

We note that our approach can encounter difficulties in various examples. First of all, we, for simplicity, do not reparametrize during the flow, so it is possible, with complex flows, that the parametrization will break down, with very large or very small $|\gamma_s|$ values. This is a well-known issue in front tracking. We do note that parametrizations will not degenerate too quickly since we are only dealing with normal velocities.

Also, sometimes our condition of $|rH| < 1$ can be violated during the descent flow.

This means the worm is trying to have its sides pass through themselves in an effort to reduce the effect of caustics on its skin. This nonphysical situation usually reveals itself with CFL restrictions of Δt_k going to zero in our algorithm [5].

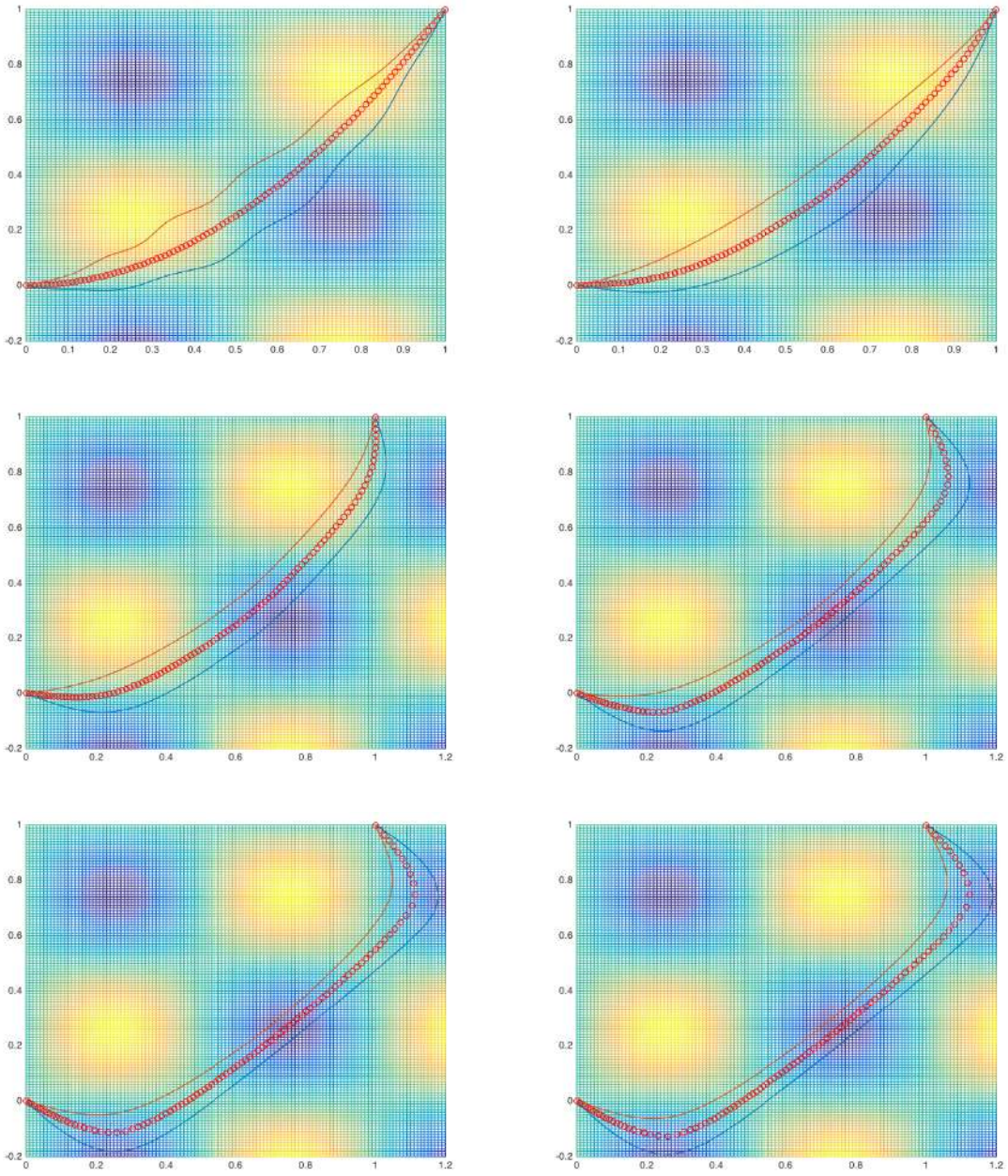

Figure 2: In this figure, we show initial worm shape in the top left, then subsequent worm shapes computed by our algorithm at time steps $1,000$, $5,000$, $10,000$, $15,000$, and finally, the converged worm shape at time step $50,000$ in the bottom right. The background colors pertain to the amount of caustic material in the solution, with high amounts in yellow and low amounts in purple.

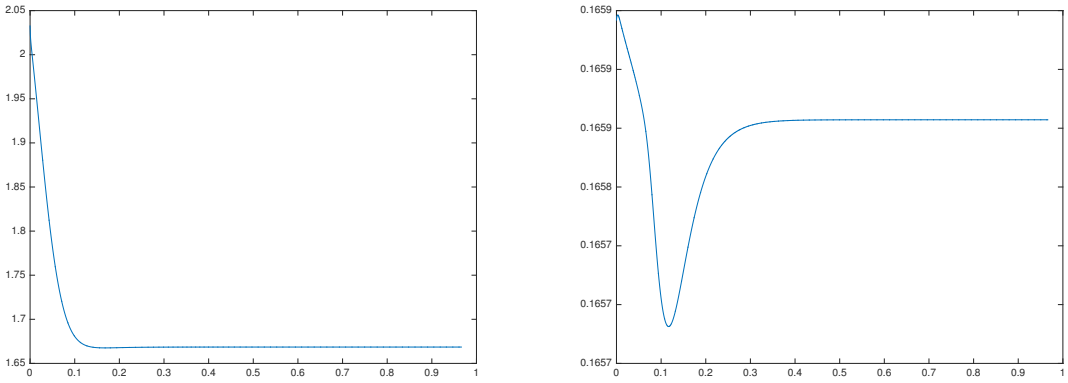

Figure 3: The figure on the left shows the values of the energy plotted against time, for a total of $50,000$ time steps. The figure on the right shows the enclosed area of the worm during these times.

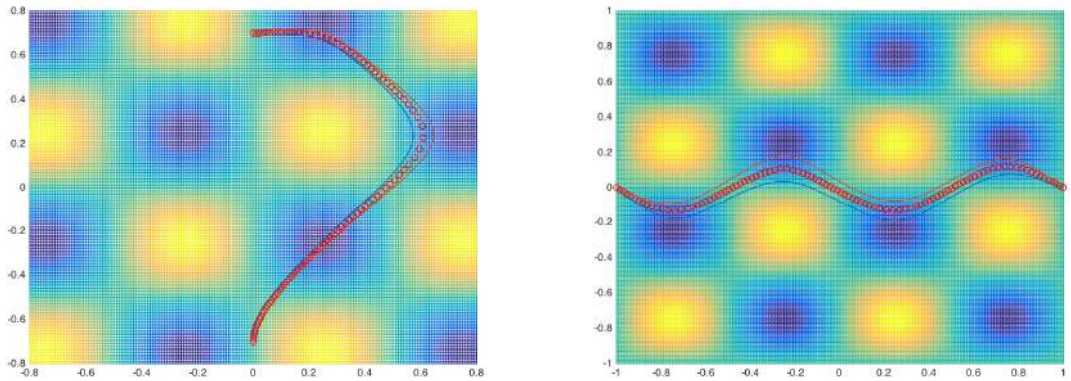

Figure 4: This figure shows two optimal worm shapes, with different endpoints and enclosed areas, computed by our algorithm.

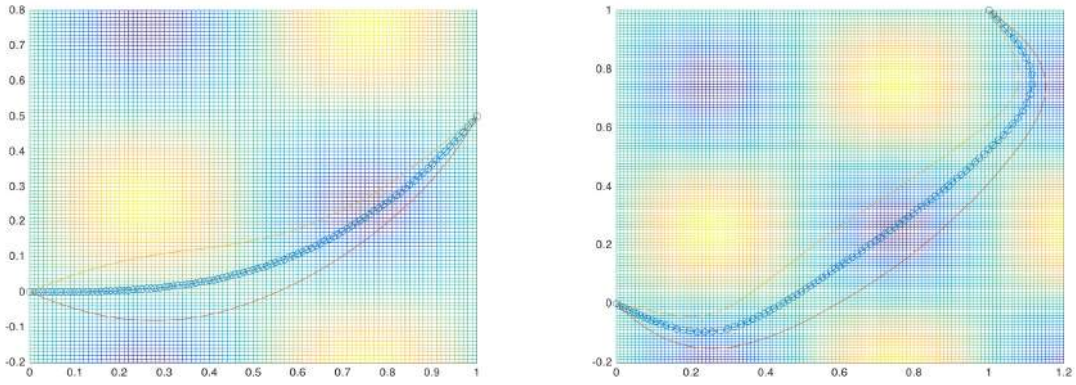

Figure 5: Left figure shows the case when γ is fixed, and right figure shows the case when r is fixed

Finally, we do not technically have a constraint on $r > 0$, even though the worm shape often does not make physical sense otherwise. We have encountered some examples where r does become zero and negative during the flow of the worm shape, thus invalidating the results of our algorithm.

6 Conclusion

In this work, we study the optimal shapes of flatworms when they are exposed to caustic solutions. We hypothesize that a flatworm attempts to minimize its surface area in order to avoid touching a caustic solution but at the same time naturally conserves its body volume. Since our investigation is confined to two dimensions, this conservation means that body area should be fixed. Thus we model the worm to vary its shape about the central axis of its body with the area constraint. We take energy methods from variational calculus and derive Euler-Lagrange Equations, and then we write descent-flow for our energy. With the area constraint, we find Lagrange Multipliers and then use a finite difference scheme for space and time. We implement our methods using Matlab to run simulations in order to check our results. The resulting solutions to the PDEs derived show in succinct form the ways flatworms respond in changing their shape in a caustic environment and how their dynamics correspond to the isoperimetric inequality. For future work, we can consider implementing more conditions, such as varying the type of caustic material to which the worm is exposed. Furthermore we expect to write a more general model in three dimensions that is applicable for different types of worms such as roundworms.

7 Acknowledgment

This work was supported in part by the National Science Foundation (NSF) through the grants DMS-1319731 and DMS-1620487 (L.-T. C. and B. L.). The authors thank Dr. Hsiao-Bing Cheng for helpful discussions.

8 Appendix A: Directional derivative

$G_{WP_\pm,\gamma,\pm}$

$$
\begin{aligned}
&\frac{d}{d\epsilon}\Big|_{\epsilon=0}\int_a^b C(\gamma+\epsilon\tilde{\gamma}\pm rn)\sqrt{(1\pm rH(\gamma+\epsilon\tilde{\gamma}))^2|\gamma'+\epsilon\tilde{\gamma}|^2+(r')^2}\;ds\\
&=\pm\int_a^b\frac{C_\pm}{D_\pm}((1\pm rH)r\tilde{H}|\gamma'|^2+(1\pm rH)^2\gamma'\cdot\tilde{\gamma}')ds+\int_a^b D_\pm(\nabla C_\pm\cdot\tilde{\gamma})ds\\
&\quad\pm\int_a^b D_\pm r\tfrac{\nabla C_\pm}{|\gamma'|}\cdot\tilde{\gamma}'^{\perp}ds\mp\int_a^b D_\pm r\tfrac{\nabla C_{pm}}{|\gamma'|^3}\cdot\gamma'^{\perp}\gamma'\cdot\tilde{\gamma}'ds\\
&=\mp\int_a^b\Big(\frac{C_\pm}{D_\pm}(1\pm rH)rn\Big)''\cdot\tilde{\gamma}\;ds\mp\int_a^b\left[\frac{C_\pm}{D_\pm}(1\pm rH)r\left(\frac{(\gamma''\cdot\tau)n}{|\gamma'|}-2H|\gamma'|\tau\right)\right]'\cdot\tilde{\gamma}\;ds\\
&\quad-\int_a^b\Big(\frac{C_\pm}{D_\pm}(1\pm rH)^2\gamma'\Big)'\cdot\tilde{\gamma}\;ds+\int_a^b D_\pm\nabla C_\pm\cdot\tilde{\gamma}\pm\int_a^b\left(D_\pm\frac{r(\nabla C_\pm)^\perp}{|\gamma'|}\right)'\cdot\tilde{\gamma}\\
&\quad\pm\int_a^b\left(D_\pm\frac{r\nabla C_\pm\cdot n}{|\gamma'|}\tau\right)'\cdot\tilde{\gamma}\;ds\pm\Big[\frac{C_\pm}{D_\pm}r'(n\cdot\tilde{\gamma})\Big]_a^b+\Big[\frac{C_\pm}{D_\pm}\gamma'\cdot\tilde{\gamma}\Big]_a^b
\end{aligned}
$$

where $\tilde{H}$ is given by

$$\tilde{H}=-\frac{\tilde{\gamma}''\cdot n}{|\gamma'|^2}+\frac{\gamma''^{\perp}\cdot\tilde{\gamma}'}{|\gamma'|^3}+3\frac{\gamma''\cdot n}{|\gamma'|^4}\gamma'\cdot\tilde{\gamma}'=-\frac{\tilde{\gamma}''\cdot n}{|\gamma'|^2}+\frac{\gamma''^{\perp}\cdot\tilde{\gamma}'}{|\gamma'|^3}+3\frac{\gamma''\cdot n}{|\gamma'|^3}\tau\cdot\tilde{\gamma}'$$

Following are some useful properties used above:

$$n'=\tau^{\perp\prime}=\tau'^{\perp}=|\gamma'|(-Hn)^{\perp}=H\gamma'$$

9 Appendix B: Descent flow

We write descent flow as following:

$$
\begin{aligned}
&-\frac{G_{WP_{\pm},\gamma}}{|\gamma_s|}\cdot n\\
&=\pm\tfrac{1}{|\gamma_s|}(\tfrac{C_\pm}{D_\pm}(1\pm rH)rn)_{ss}\cdot n\pm\tfrac{1}{|\gamma_s|}\tfrac{C_\pm}{D_\pm}\tfrac{r}{|\gamma_s|}(\gamma_{ss}^{\perp}+3(\gamma_{ss}\cdot n)\tau)_s\cdot n\\
&\quad-\tfrac{1}{|\gamma_s|}D_\pm\nabla C_\pm\cdot n\mp\tfrac{1}{|\gamma_s|}\left(D_\pm r\tfrac{\nabla C_\pm}{|\gamma|_s}\right)_s\cdot\tau\mp\tfrac{1}{|\gamma_s|}\left(D_\pm r\tfrac{\nabla C_\pm\cdot n}{|\gamma|_s}\tau\right)_s\cdot n\\
&=\pm\tfrac{1}{|\gamma|_s}\left(\tfrac{C_\pm}{D_\pm}r\right)_{ss}\mp\tfrac{1}{|\gamma|_s}\tfrac{C_\pm}{D_\pm}rH^2|\gamma|_s^3H^2-\tfrac{1}{|\gamma|_s}\tfrac{C_\pm}{D_\pm}(1\pm rH)^2|\gamma_s|^2H-\tfrac{1}{|\gamma_s|}D_\pm\nabla C_\pm\cdot n\\
&\quad\mp\tfrac{1}{|\gamma_s|}\left(D_\pm r\tfrac{\nabla C_\pm}{|\gamma|_s}\right)_s\cdot\tau\mp\tfrac{1}{|\gamma_s|}\left(D_\pm r\tfrac{\nabla C_\pm\cdot n}{|\gamma|_s}\tau\right)_s\cdot n\\
&=\pm\frac{1}{|\gamma_s|}\left(\frac{C_\pm}{D_\pm}(1\pm rH)r\right)_{ss}\pm\frac{1}{|\gamma_s|}\left(\frac{C_\pm}{D_\pm}(1\pm rH)r\frac{\gamma_{ss}\cdot\tau}{|\gamma_s|}\right)_s\\
&\quad-\frac{C_\pm}{D_\pm}(1\pm rH)H|\gamma_s|-(1\mp rH)D_\pm\frac{\nabla C_\pm\cdot n}{|\gamma_s|}\mp\frac{1}{|\gamma_s|}\left(rD_\pm\frac{\nabla C_\pm}{|\gamma_s|}\right)_s\cdot\tau
\end{aligned}
$$

References

[1] R. Courant, D. Hilbert, *Methods of Mathematical Physics*,Interscience Publishers, 1953.

[2] S.J.Farlow. *Partial Differential Equations for Scientists and Engineers*, Dover, 1993

[3] I.M. Gelfand, S.V. Fomin, *Calculus of Variations*, Dover, 2000.

[4] C.Lanczos. *The Variational Principles of Mechanics, 4th edition,*, Dover 2012

[5] S.Larsson, V. Thomee, *Partial Differential Equations with Numerical Methods*, Springer, 2009.

[6] S.Osher, R.Fedkiw, *Level Set Methods and Dynamic Implicit Surfaces*, Springer, 2003.

[7] W.A.Strauss, *Partial Differential Equations, 2nd edition*, Wiley, 2008.

[8] G.Tryggvason, B.Bunner, D.Juric, W.Tauber, S.Nas, J.Han, N. Al-Rawahi,Y.-J.Jan, A Front Tracking Method for the Computations of Multiphase Flow, *J.Comput. Phys.V.*169, 708-759, 2001.

[9] S.O. Unverdi, G. Tryggvason, A Front-Tracking Method for Viscous, Incompressible, Multi-Fluid Flows, *J. Comput. Phys.* 100, 25-37, 1992

[10] S.Werner, J.C.Rink, I.H.Riedel-Kruse, B.M.Friedrich Shape Mode Analysis Exposes Movement Patterns in Biology: Flagella and Flatworms as Case Studies, *PLoS ONE*9(11):e113083

[11] S.E.Wilson-Sanders. Invertebrate Models for Biomedical Research, *ILAK J.*52: 126-152, 2011

[12] Y.L. Zhang, K.S. Yeo, B.C. Khoo, C. Wang, 3D Jet Impact of Toroidal Bubbles *J. Comput. Phys.* 166, 336-360, 2001